Variability of Cygnus X-1
Spectral evolution 2005

Moritz Böck

guided by Prof. Dr. Jörn Wilms, Dr. Karl Remeis-Sternwarte Bamberg
(Dated: March 2007)

The spectral evolution of the galactic black hole candidate Cygnus X-1 was analyzed. Using the data obtained by observations, which were taken with the Rossi X-ray Timing Explorer, the X-ray spectrum was modeled. Data is available up to december 29th in 2005 and the covered energy range is 4-200 keV. It turned out, that Cyg X-1 spent the second half of 2005 in a hard state. The obtained relations between the fit parameters were consistent with the results of the observation from 1999-2004 (Wilms et al. [1]).

Contents

I. INTRODUCTION

The issue of this project was to continue the long-term observation of the black hole X-ray binary Cygnus X-1, initiated by J. Wilms et al. [1]. In their work, about 200 observations were considered in order to analyze the spectral evolution of Cygnus X-1 in the space of time between 1999 and 2004. The data was obtained by the Rossi X-ray Timing Explorer (*RXTE*) and the spectra were fitted with the help of the program *XSPEC* [12]. In this work, 40 observations (also taken with *RXTE*) were evaluated. 15 of them were from 2005, while the others (2002-2004) were used to compare the results with the long-term observation. Instead of *XSPEC*, *ISIS* [11] was used here. As expected, the results were consistent.

The main task of this project was, to automatize the fitting process of the spectra. Therefore an algorithm was created, which loads the data of an observation, uses *ISIS* to fit the spectrum and to calculate the confidence interval for each parameter and continues this procedure with the next observation. It was necessary to find the best fitting strategy, i.e. the best order of freezing parameters at certain values, while varying other ones and then repeating the process in different combinations, in order to approach the best fit. Varying all 11 (13 with the blackbody radiation of the accretion disk) parameters at once, would only yield a side minimum and most likely unreasonable values for the fit parameters. This will be discussed further in section IV.

In the following, the theoretical background of black hole binaries is outlined. Afterwards the data analysis and the modelling of the spectra are explained and finally the results are presented.

II. BLACK HOLE X-RAY BINARIES

A. Black Holes

Black holes are quite famous today. A black hole is an object with such a large mass, that even light cannot escape from it due to its enormous gravity. It is enclosed by the event horizon, a mathematical surface, which is characterized by the fact that no information, like electromagnetic radiation can leave it. The escape velocity at the event horizon is equal to the speed of light. For a nonrotating black hole, this surface is given by a sphere with the radius:

$$R_{\mathrm{S}} = 2GM/c^2$$

Where R_S is called the *Schwarzschild radius*. (M is the mass of the black hole, G is the Gravitational constant and c the speed of light.) The event horizon is a kind of barrier, no information from the inside can reach the outside. Therefore it is impossible to study a black hole directly. But its existence can be proven, by observing the behaviour of surrounding objects. A black hole can be characterized by its mass, its angular momentum and the electric charge.
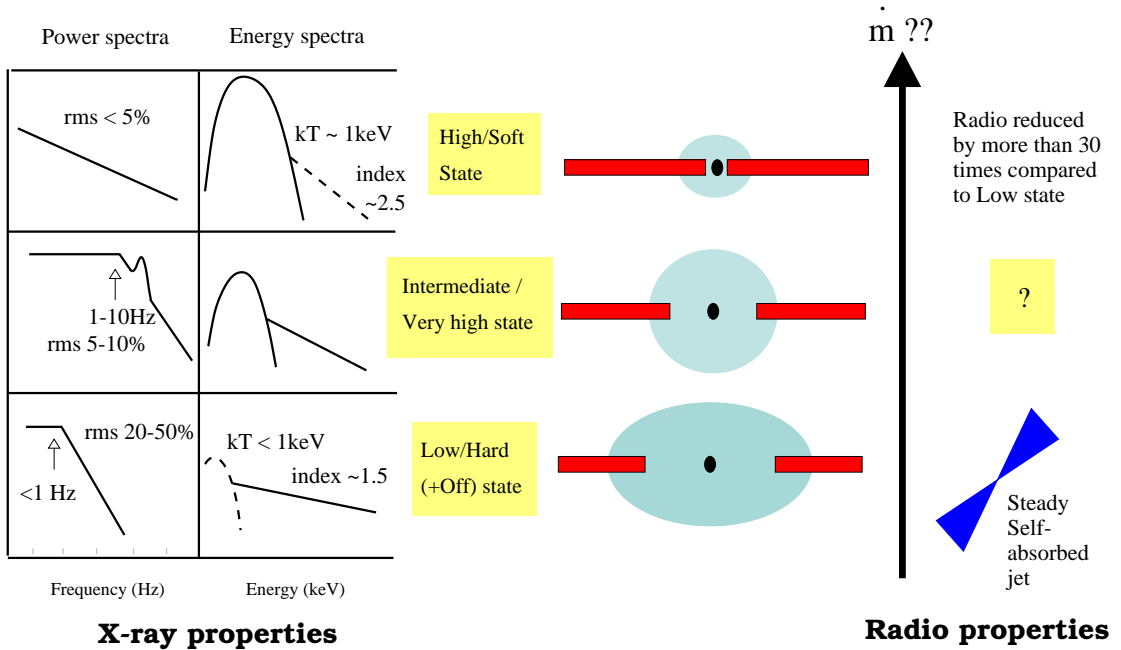
FIG. 1: Schematic illustration of the most important states, with the corresponding spectral shape, accretion rate $\dot{m}$ and geometry of disk and corona. (Picture from [9], Fig. 4)

B. Accretion

A massive object can grow by gravitationally attracting matter. This phenomenon is called accretion. Due to the conservation of angular momentum, the attracted matter is inhibited to fall radially onto the massive object, which is a black hole in this case. For this reason, the accretion disk (or disc) develops. Every particle in the disk is approximately on a Keplerian orbit, but viscosity causes a transfer of angular momentum between the particles. Thus inner particles lose angular momentum and approach the black hole on spiral trajectories. The different velocities within the disk ($\Omega_{\mathrm{K}}(R) \approx \sqrt{GM/R^3}$) and friction cause a heating of the disk. In this manner, parts of the gravitational energy can be emitted in form of electromagnetical radiation. The temperature of the disk decreases outwards, it is proportional to $R^{-3/4}$ (see [10]). Accretion onto a compact object is the most efficient mechanism of converting mass into radiation energy.

The maximal stationary luminosity of an object of mass M, which radially (spherically symmetric) accretes ionized gas, can be calculated by assuming, that the radiation pressure and the gravitational force are equal. It is called Eddington luminosity and given by (calculation: see [10]):

$$L_{\mathrm{Edd}} \approx 1.3 \cdot 10^{38} \mathrm{erg\ s}^{-1} \cdot \frac{M}{M_\odot} = 3.3 \cdot 10^4 \cdot \frac{M}{M_\odot} L_\odot$$

Where $M_\odot$ is the solar mass and $L_\odot$ its luminosity.

C. States

The states, which are introduced in this section, classify the behavior of a Black Hole Binary (BHB). A BHB is a binary, which consists of a black hole and a secondary star. In a binary, there can be mass-exchange. In this case, the black hole accretes matter from its companion star. There is a broad spectrum of different accretion rates for different binaries. Also a single BHB can show a large variability in time. There are even systems with a characteristic behaviour. The varying kinds of accretion are the explanation for the different states. The states of BHBs are classified mainly by the properties of their X-ray spectra. One differentiates between the high (soft) state, the intermediate state and the low (hard) state (see Fig. 1). There was even a quiescent and a very high state introduced (see [3], Fig. 4.1). In this work, it was sufficient to restrict oneself to the hard and soft state. These two states will be discussed in detail now. A
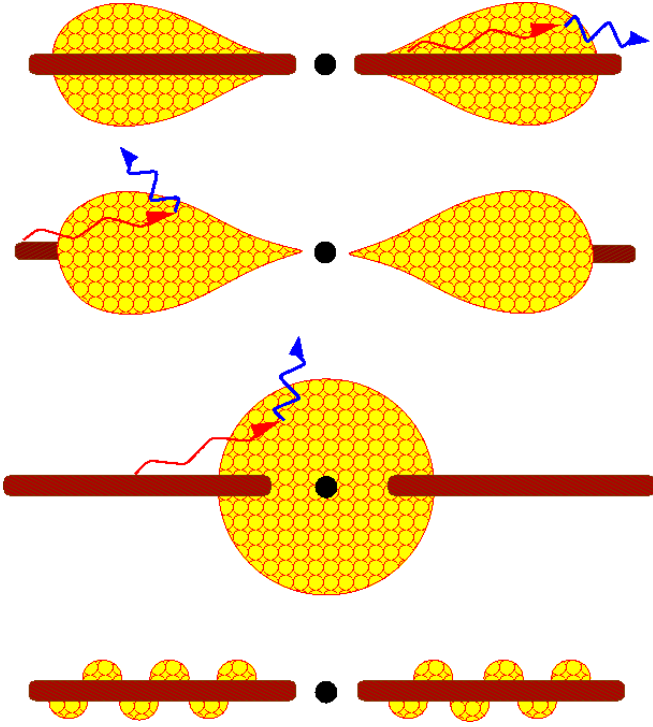
FIG. 2: Different sketches, which illustrate possible geometries of the disk and the corona (and the Comptonization process). (Picture from [13])

inner disk radius is larger. Therefore the disk is colder and there are much less seed photons. The corona is now photon-starved. The result is, that the Comptonization yields photons with higher energies. It is now easy to understand, that a hard state spectrum is characterized by a large powerlaw component with a small photon index (≤ 2.1), whereas the thermal radiation is relatively weak. It could be completely neglected in this work, because only energies from 4-200 keV were considered. With several percents of L_{Edd}, the broadband luminosity of a hard state is much smaller than that of a soft state.

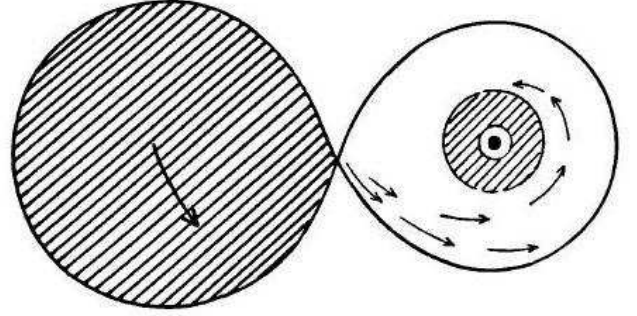There are binaries, which are most often in the soft

FIG. 3: Here the Roche lobe overflow is shown. The star fills its Roche lobe and the mass-exchange rate is large. (Picture from [4])

soft state spectrum is dominated by a soft, thermal component, the black body radiation coming from the disk. It has a temperature in the order of 1 keV. The broadband luminosity is relatively large, it can even exceed 50% of the Eddington luminosity. There is also a power law component, which becomes important at higher energies. The photon index (see section IV C) is large. It can be shown (see [10]) that Comptonization causes a power law spectrum. This process works as follows: photons that come from the disk, the so-called seed photons, are scattered several times by electrons in the corona. The corona consists of a hot (optical thin) plasma, which has a temperature of about 100-300 keV. Because its temperature is larger than the energy of the incoming photons, the photons gain energy by Comptonization, while the corona is cooled. Assuming a Maxwellian velocity distribution of the electrons, it can be shown, that the average relative energy change of a photon is given by (see [4], Eq. 1.16):

$$\frac{\Delta E}{E} \approx \frac{4k_{\mathrm{B}}T_e - E}{m_e c^2}$$

Where $E = h\nu$ is the energy of the incoming photon, and T_e and m_e are the temperature and the mass of the electrons, respectively. Fig. 2 illustrates different geometries of the corona. In the case of a soft state, the accretion rate is high and the disk reaches close to the black hole, thus thermal radiation becomes important. The situation is different for the hard state. Here, the

state, while others spend most of their time in the hard state. One important reason for this behavior can be seen by considering the *Roche lobe*. This is the volume, which is enclosed by the Roche surface. The smallest common equipotential surface around the binary system with one point (inner Lagrangian point) that seperates the volume into the Roche lobe of the star and the one of the black hole (see Fig. 3). If the star has the size of
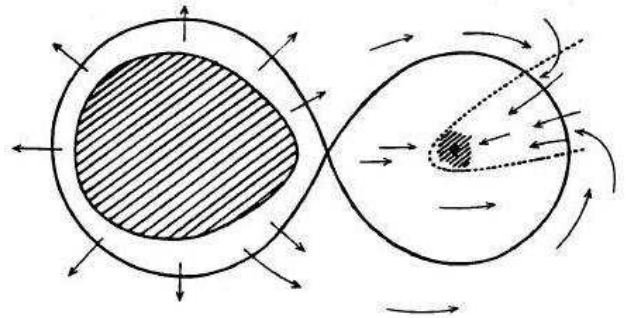

FIG. 4: The star is smaller than its Roche lobe, wind accretion is important. (Picture from [4])

its Roche lobe (see Fig. 3), matter in the proximity of the inner Lagrangian point can easily flow from the star to the black hole. This process is called Roche lobe overflow. The accretion rate can be very large in this case. Thus, such systems are often found in a soft state. If the

star is smaller than its Roche lobe, the black hole accretes mostly stellar wind. The wind accretion is illustrated in Fig. 4.

D. Cygnus X-1

Cygnus X-1 (4U 1956+35) is a black hole binary (BHB). It is a mass-exchange binary that contains an accreting black hole and a secondary star. Cyg X-1 is a so-called high-mass X-ray binary (HMXB), because the secondary (HD 226868) is a massive O9.7 star, with a mass of about 18 $M_\odot$ (see [8]). The mass of the black hole is assumed to be about 10 (6.9-13.2 [3]) solar masses. Cyg X-1 is an interesting object, because it is one of the brightest hard X-ray sources and it has shown extreme variability in the radiation intensity. In the case of Cyg X-1, the wind accretion is important, because O/B stars have a large mass loss rate, due to stellar wind. The variability can be explained by a changeable accretion rate. It is assumed, that Cyg X-1 is in a mixture of wind accretion and Roche lobe overflow [15].

III. DATA

A. The Rossi X-ray Timing Explorer (RXTE)

The used data was obtained by the Rossi X-ray Timing Explorer (Fig. 5). RXTE is a large X-ray detector, which was launched on 1995 December 30. During the last 11 years, its observations have been very helpful to find properties of black holes, neutron stars and white dwarfs. It covers an energy range of 2-250 keV. This range is achieved by using different instruments that are effective for certain energies. The Proportional Counter Array (PCA) has the largest total net area (6250 cm^2) and covers the energy range 2-60 keV. The High Energy Timing Experiment (HEXTE) works well for energies from 15 up to 250 keV. PCA and HEXTE have the same 1° field of view, while RXTE's third instrument, the All-Sky-Monitor (ASM), is compromised of three wide field proportional counters that are mounted on a rotating boom. It scans 80% of the sky every 90 minutes an has an energy range of 2-10 keV. In this project, the energy range of the applied data was 4-20 keV (PCA) and 20-200 keV (HEXTE).

B. Data Analysis

In order to get physical properties of the observed source, one wants to find its photon flux density $F_S(E)$ [photons/cm^2/s/keV]. The problem is that the measured flux is different to the flux, which comes from the source. The measurement process can be described mathemati-
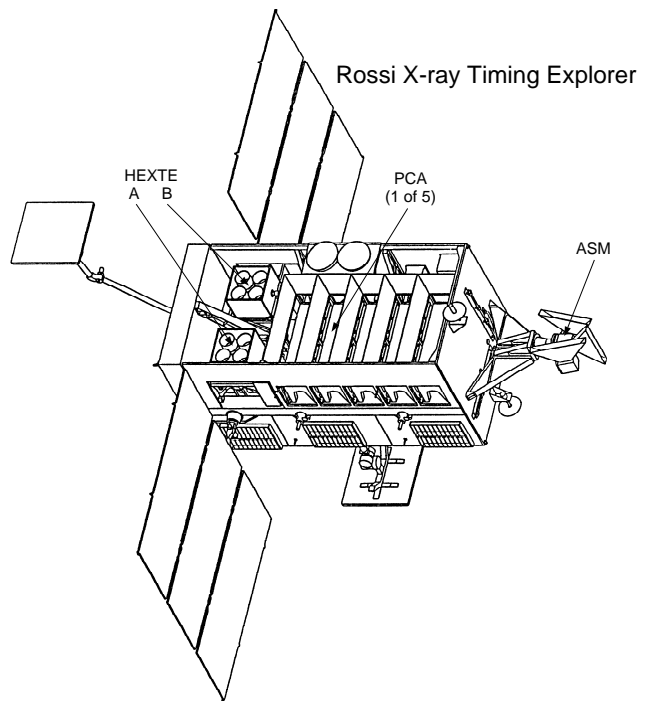

FIG. 5: The Rossi X-ray Timing Explorer (RXTE). (Picture from [14])

cally by:

$$C_D(E) = \int_0^\infty R(E, E')A(E')(F_S(E') + B(E'))dE' \quad (1)$$

with

- $C_D(E)$: count rate of the detector
- $A(E')$: effective detector area
- $F_S(E')$: photon flux density of the source
- $B(E')$: background photon flux density
- $R(E, E')$: detector response (probability to detect a photon with energy E' as a photon with energy E)

An ideal detector corresponds to $R(E, E') = \delta(E - E')$. Additionally the energy of the photon is not measured exactly, because the energy range of a the detectors is divided into several bins. Each of them covers a certain energy band (E_i, E_{i+1}). Subtracting the background and descretizing Eq. (1) yields:

$$N_S(E_i) = T \sum_{i=0}^{n_{bin}} A(E_i)R(E, E_i)F(E_i)\Delta E_i \quad (2)$$

Here, $N_S(E_i)$ is the total number of "source photons", which are detected in the bin n_i, T is the exposure time
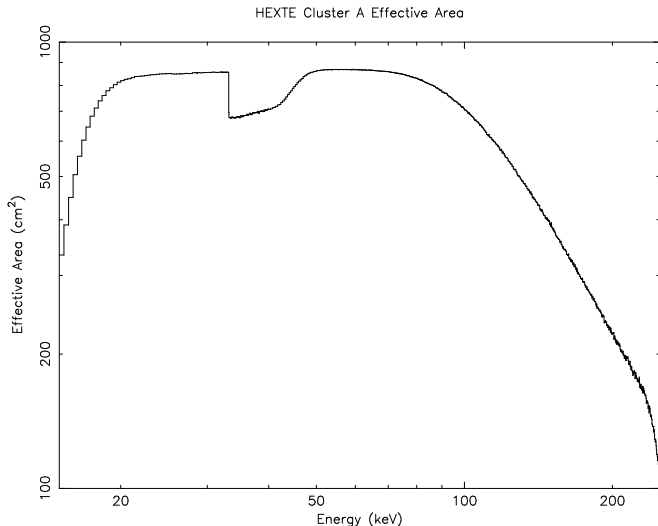
FIG. 6: The effective area of the detector *HEXTE* A.

and $\Delta E_i = (E_{i+1} - E_i)$. Knowing the flux, the count rate can be calculated, whereas the inverse calculation is problematic. For this reason the χ^2-minimization approach is applied:

1. A model $F_M(E; p_1, p_2, ...p_k)$ for the spectrum of the source is considered. $\{p_1, p_2, ...p_k\}$ is a set of parameters.

2. The model count rate $N_M(E_i)$ is calculated, by substituting $F_M(E; p_1, p_2, ...p_k)$ into Eq. (2)

3. χ^2 is calculated:

$$\chi^2(p_1, p_2, ...p_k) = \sum_{E_i} \frac{(N_S(E_i) - N_M(E_i))^2}{\sigma(E_i)^2}$$

σ is the measurement uncertainty.

4. The parameters are varied, until χ^2 is minimal.

For this procedure it is useful to utilize programs like *ISIS* or *XSPEC*. In this project, *ISIS* [11] was used.

IV. MODELING THE SPECTRUM OF CYGNUS X-1

A. The fit function

The target is to find a model for the spectrum of Cyg X-1, which fits very good to the measured data without using too many parameters. It has turned out [1], that the best fits for BHB spectra can be achieved by using a broken powerlaw with an exponential cutoff. The complete fit function, reads as follows:

$$F_M(E) = \text{phabs}(E)*\text{constant}(\text{Isis\_Active\_Dataset})*$$
$$(\text{bknpower}(E)*\text{highecut}(E)+\text{egauss}(E))$$

The function *constant(Isis_Active_Dataset)* is used to scale the *PCA* (4-20 keV) and the *HEXTE* (20-200 keV) data to an equal level. One data set is multiplied by a constant factor, due to different calibrations. The other components of the fit function will be discussed in detail now.

B. Photoelectric absorption

In this process, a photon interacts with the interstellar medium. Photons can be absorbed, when they collide with atoms and transfer their energy to an orbital electron. The absorption rate depends on the energy of the photon and the nature of the atom. For hydrogen, the most abundant element in the interstellar medium, the energy of the X-ray photon is much larger than the binding energy and the electron is ejected at high velocity. The cross section is larger for X-rays with lower energies. For higher energies it becomes more important, when the number of atoms with higher atomic number increases. In our the model, the photoelectric absorption is mathematically approximated by the function:

$$\text{phabs}(E) = \exp^{-N_\text{H}\sigma(E)}$$

Where $\sigma(E)$ is an approximated photoelectric cross section. The only paramater of this function is:

N_H equivalent hydrogen column (in units of 10^{22} atoms/cm^2)

C. Broken powerlaw

As already mentioned in section II C, the Comptonization yields a powerlaw.

$$\text{bknpower}(E) =$$
$$\begin{cases} K(E/1\text{ keV})^{\Gamma_1} & \text{for } E \leq E_\text{break} \\ K(E_\text{break}/1\text{ keV})^{\Gamma_1 - \Gamma_2}(E/1\text{ keV})^{\Gamma_2} & \text{for } E \geq E_\text{break} \end{cases}$$

For the broken powerlaw function, four parameters are used:

K the *norm* (in units of photons/keV/cm^2/s at 1 keV)
Γ_1 the powerlaw photon index for $E \leq E_\text{break}$
E_break break point for the energy in keV
Γ_2 the powerlaw photon index for $E \geq E_\text{break}$

The photon index Γ_1 is useful to distinguish hard and soft states. Hard states can be defined by $\Gamma_1 \leq 2.1$.

D. High energy cutoff

The application of an exponential high energy cutoff is justified by the fact that we assumed a Maxwellian velocity distribution for the electrons in the corona, which

N_H=1.37, Γ_1=1.94, Γ_2=1.63, E_{Break}=9.40, E_{cut}=27.63, E_{fold}=164.44, χ^2_{red}=0.92
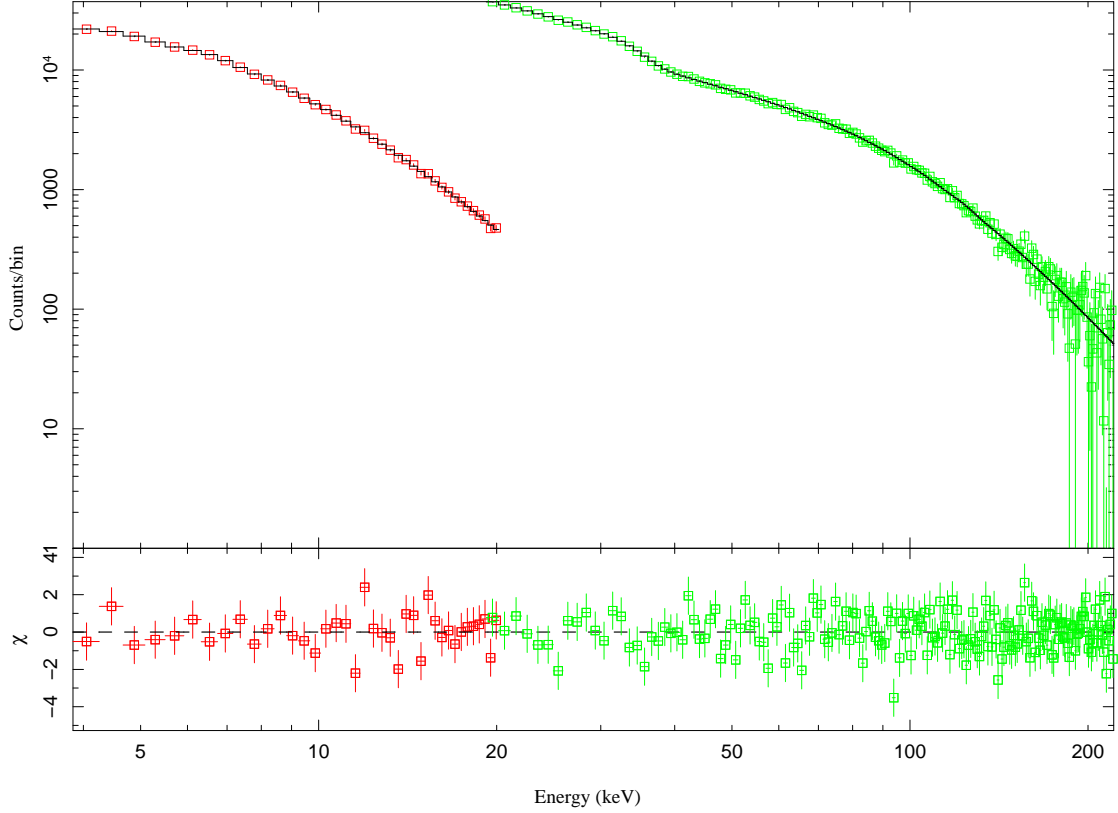
FIG. 7: A good fit for the spectrum, which was measured at november 29, 2005

has a temperature of 100-300 keV. Above a certain energy limit, the probability that the photons lose energy by compton scattering becomes significant.

$$\text{highecut}(E) = \begin{cases} 1 & \text{for } E \leq E_{\text{cut}} \\ \exp\left[(E_{\text{cut}} - E)/E_{\text{fold}}\right] & \text{for } E \geq E_{\text{cut}} \end{cases}$$

To characterize the high energy cutoff, two parameters are necessary:

E_{cut} cutoff energy in keV
E_{fold} exponential folding energy in keV

E. Gaussian line profile function

In this model, one Gaussian function is used in order to fit the Fe Kα line. The energy of this transition is 6.4 keV. The broadening of the line can be explained by the Doppler effect, caused by the high rotation velocity in the accretion disk.

$$\text{egauss}(E) = \frac{A}{\sigma\sqrt{2\pi}} \exp\left[-\frac{(E - E_0)^2}{2\sigma^2}\right]$$

The shape of a Gaussian function depends on three parameters:

A total area under the Gaussian function (in units of photons/s/cm^2)
E_0 the center of the function
σ its width

N_H=1.37, Γ_1=1.94, Γ_2=1.63, E_{Break}=9.40, E_{cut}=27.63, E_{fold}=164.44, χ^2_{red}=1.64
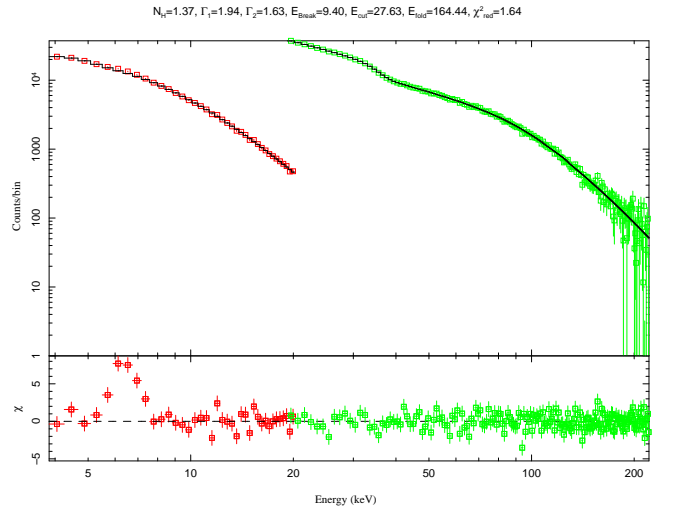
FIG. 8: The fit from Fig. 7 after removing the Gaussian line.

The contribution of the iron line to the spectrum can be seen clearly by comparing Fig. 7 and Fig. 8.
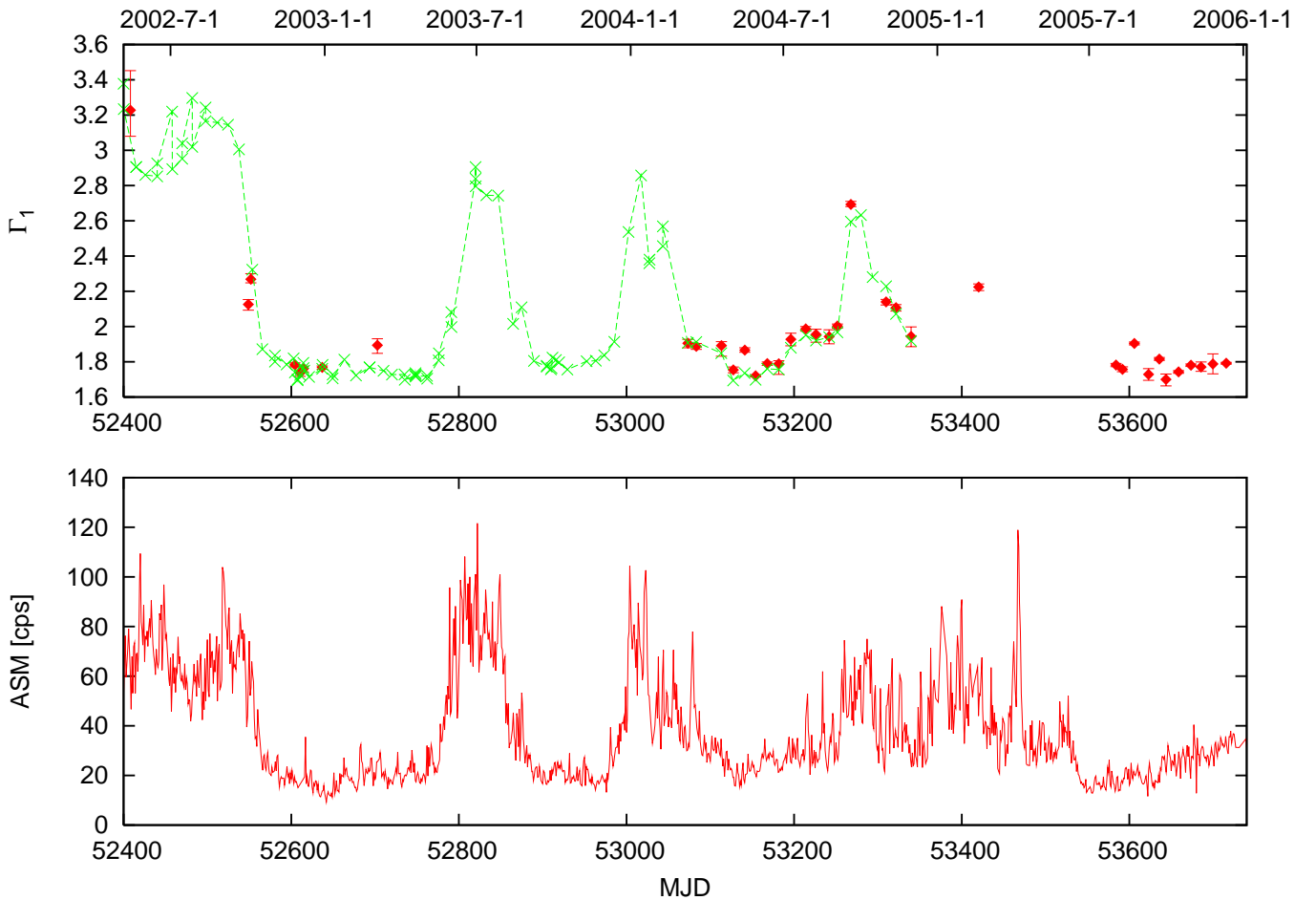
FIG. 9: The daily average ASM count rate (2-10 keV) compared to the photon index Γ_1. The values obtained in this work are the filled diamonds, while the connected crosses are the ones from the longterm observation.

F. Black body radiation

For soft states, the black body radiation of the disk has to be taken into account. Therefore the function diskbb is added to the broken powerlaw with exponential cutoff and the Gaussian function. As already mentioned, the temperature is a function of the radius: $T(R) \propto R^{-3/4}$. diskbb describes the spectrum from an accretion disk consisting of multiple black body components. Two parameters are used:

T_i temperature at inner disk radius
$K = ((R_{in}/\text{km})/(D/10\text{kpc}))^2 * \cos(\theta)$
       where R_{in} is the inner disk radius
       D the distance to the source
       and θ the angle of the disk

For the soft states of Cygnus X-1, good fits can usually be achieved with $T_{in} \approx 1\text{keV}$. Although the considered energy range is 4-200 keV, the black body radiation can not be neglected for soft states.

V. RESULTS

As mentioned above, the issue of this work was to continue the long-term observation of Cyg X-1 [1]. The behaviour of the source can be deduced by analyzing the fit parameters. In this section the parameter values for the best fits are presented. Additionally they are compared with the preceding work [1]. The displayed error bars have been calculated by applying the 90% confidence interval.

Obviously Cyg X-1 was in a hard state during the second half of 2005. The photon index was relatively small, $\Gamma_1 \approx 1.8$ (see Fig. 9). There was only one observation available for the first half of 2005. It can be seen clearly that the analysis of the data between 2002 and 2004 yielded the same results as the ones, obtained by Wilms et al. [1]. Furthermore, Fig. 9 shows the correlation between the photon index Γ_1 and the daily average flux, measured by the All-Sky-Monitor. Because the ASM is sensitive for photons with the energy 2-10 keV, Fig. 9 illustrates how the increase of the flux in the soft X-ray energy range is tied to an increase of the photon
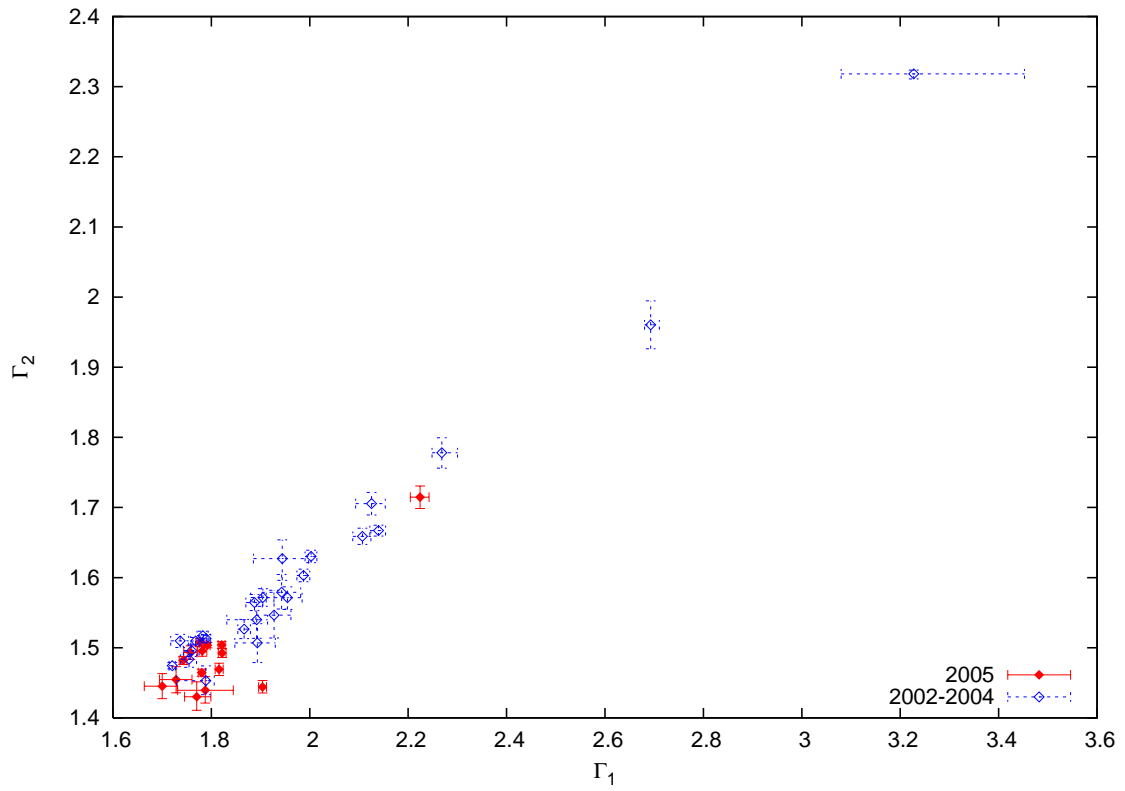
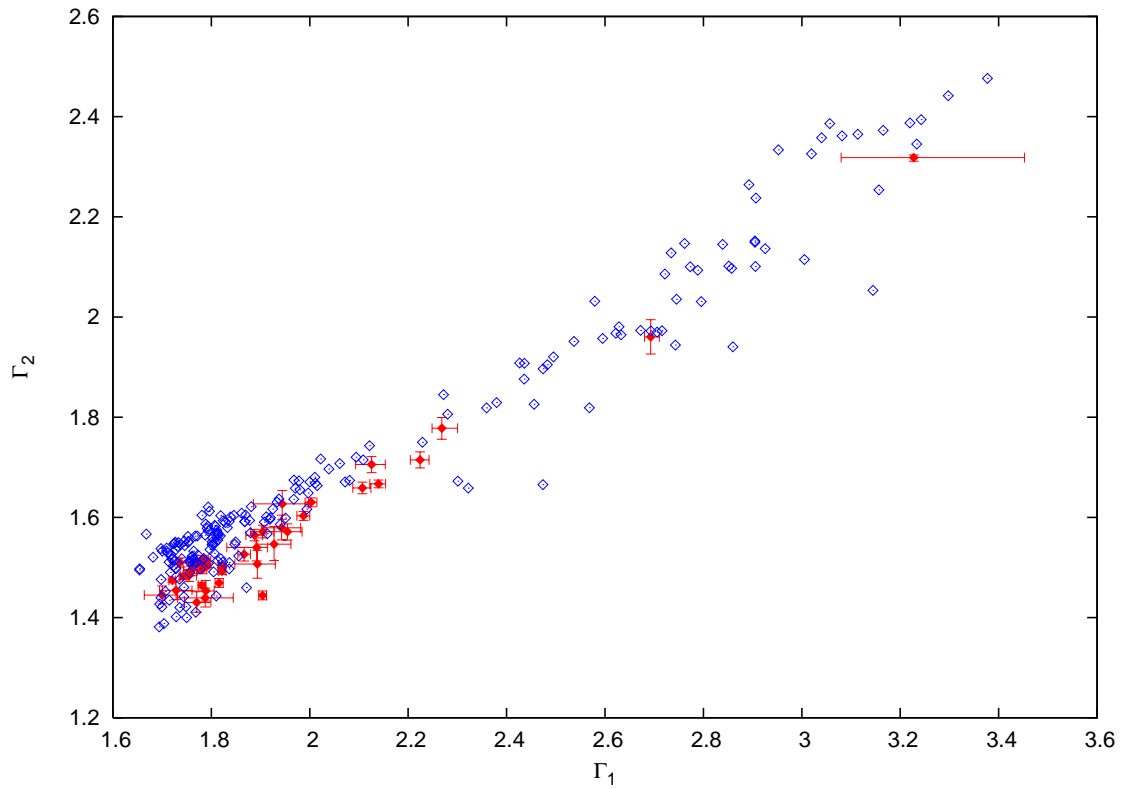FIG. 10: The relation between the two photon indices

FIG. 11: The values Γ_1 and Γ_2 from Fig. 10 compared to the ones obtained by Wilms et al. [1].
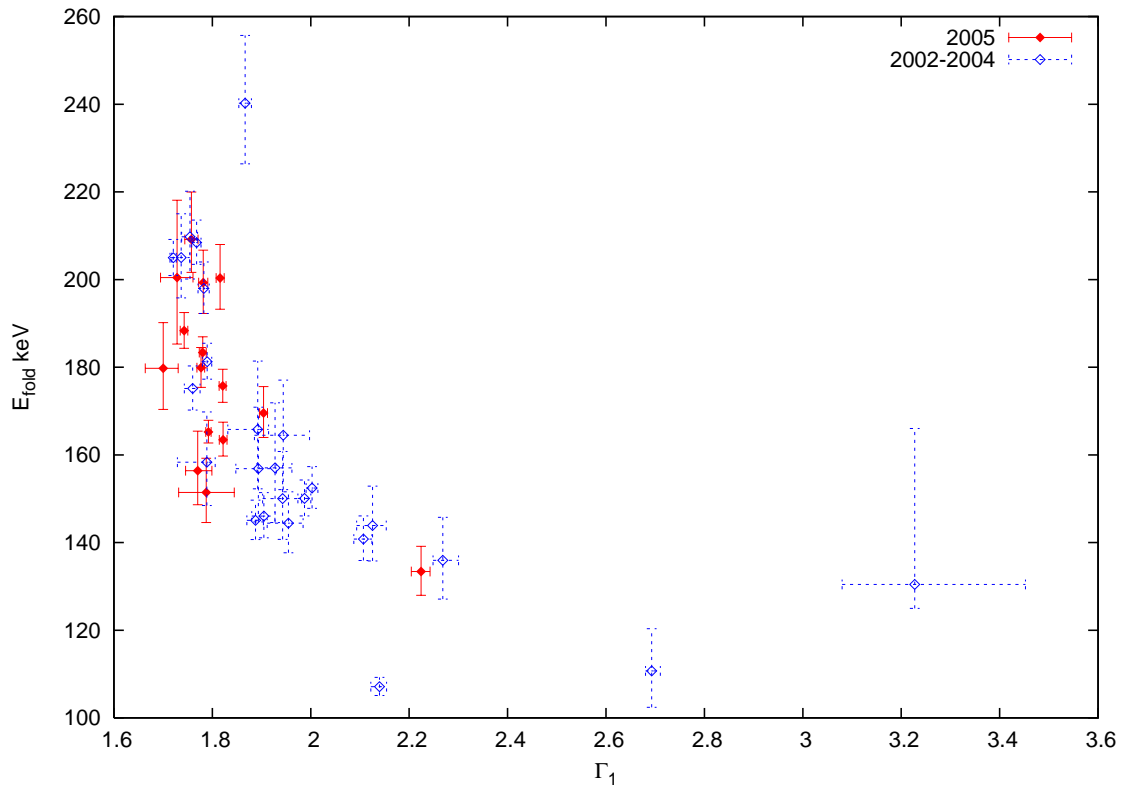
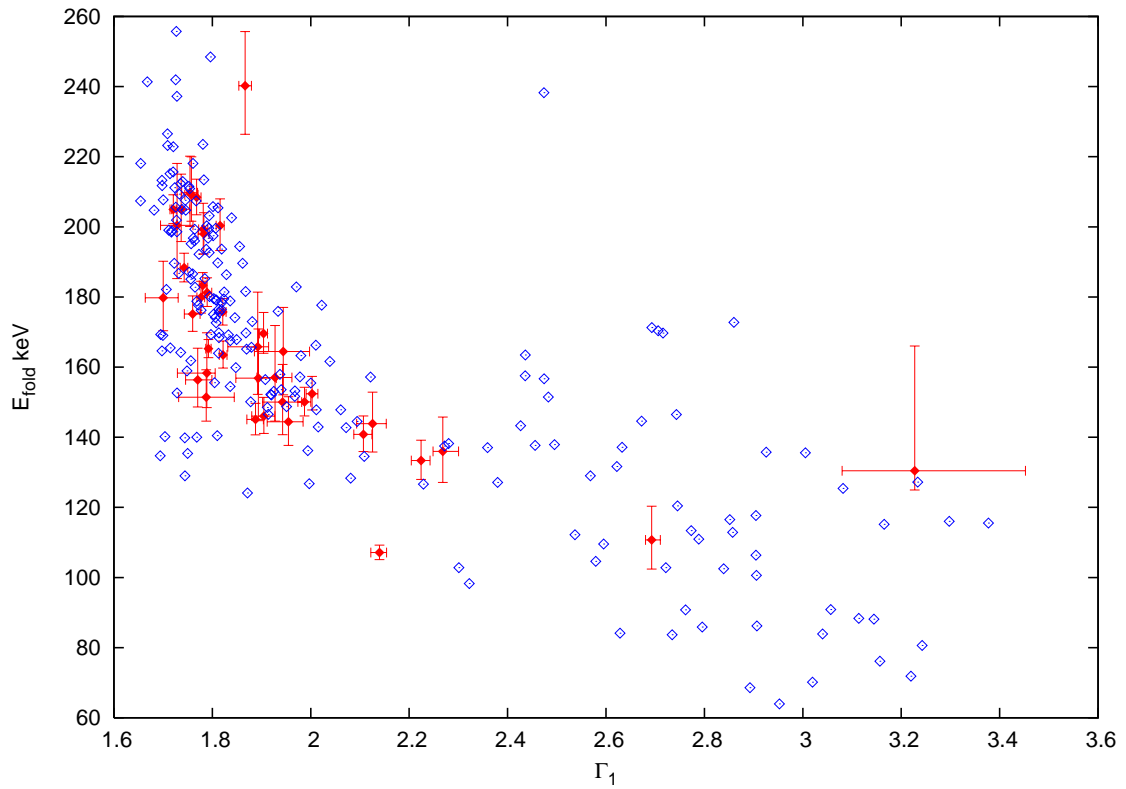FIG. 12: The relation between the folding energy of the exponential cutoff and the photon index Γ_1

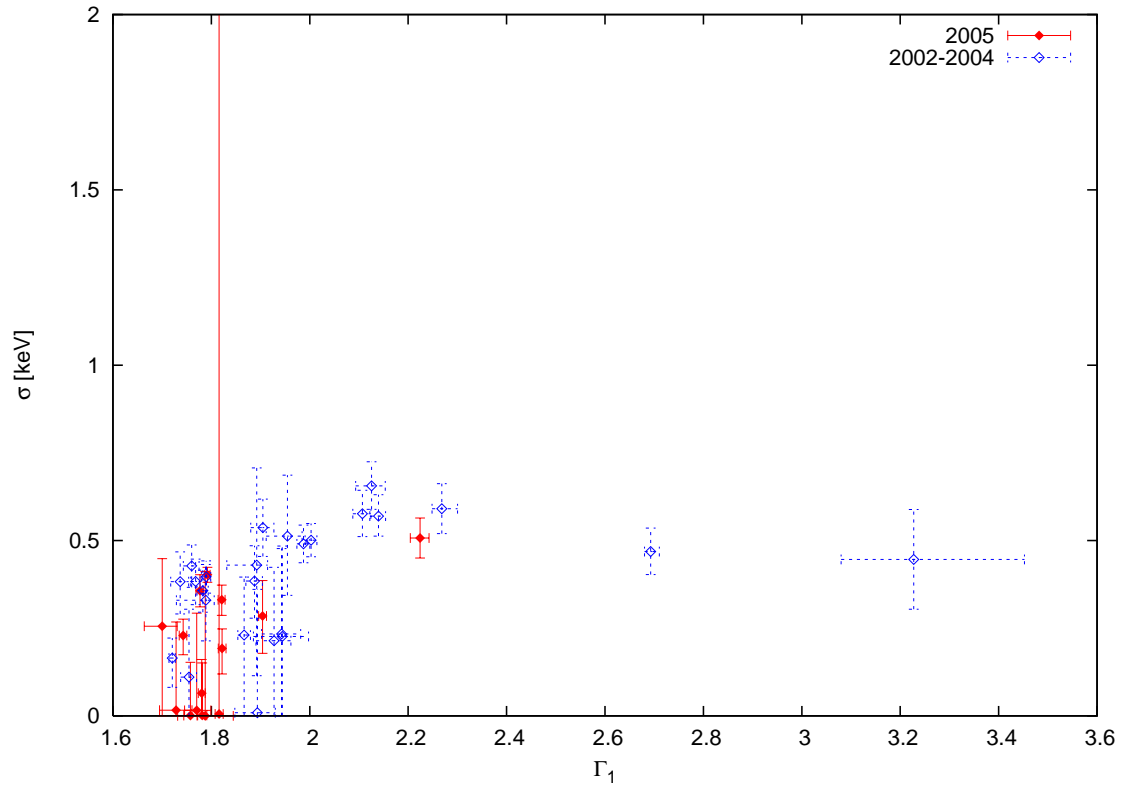FIG. 13: Fig. 12 combined with the parameter values from [1].

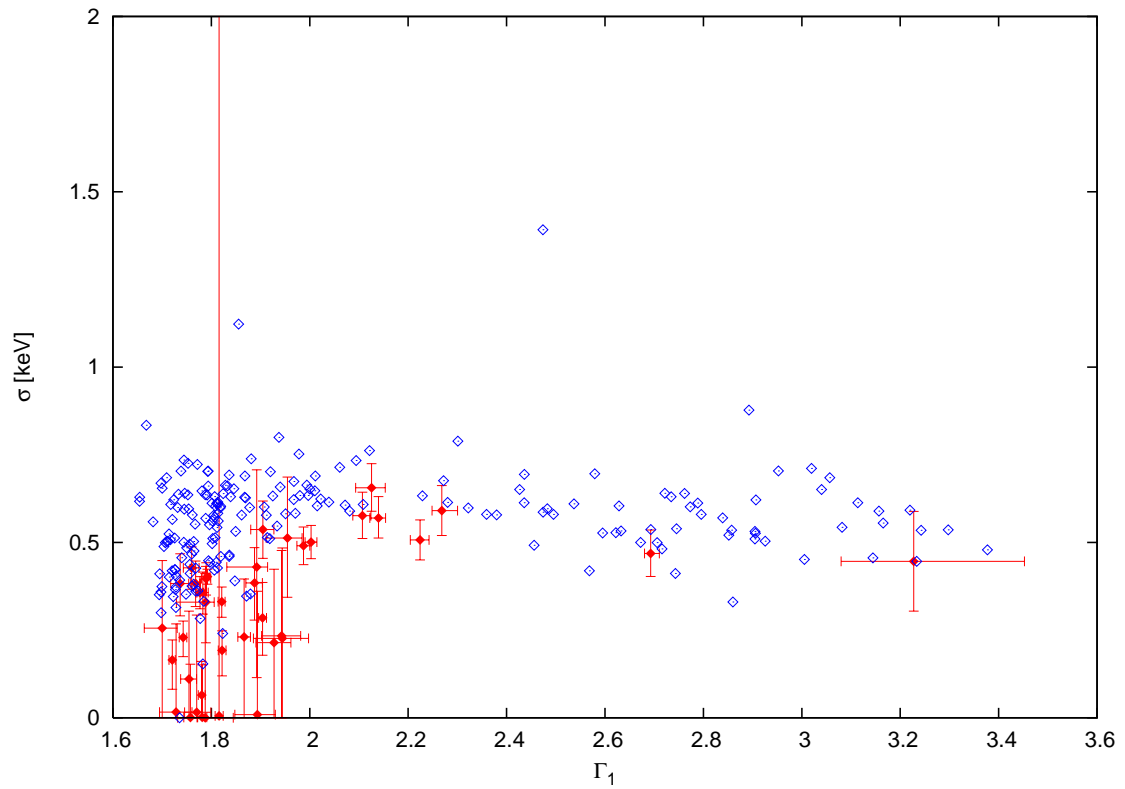FIG. 14: Obtained values for the width of the Fe Kα line.

FIG. 15: The values from Fig. 14 compared to the ones obtained by Wilms et al. [1].
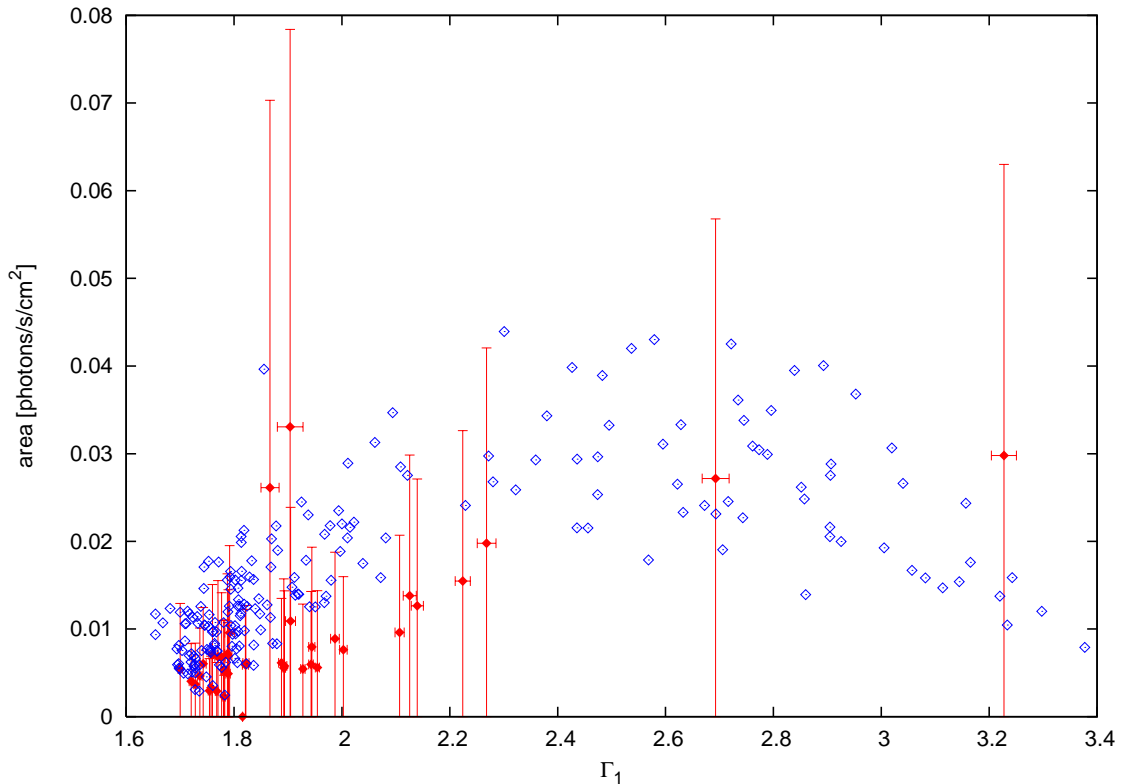
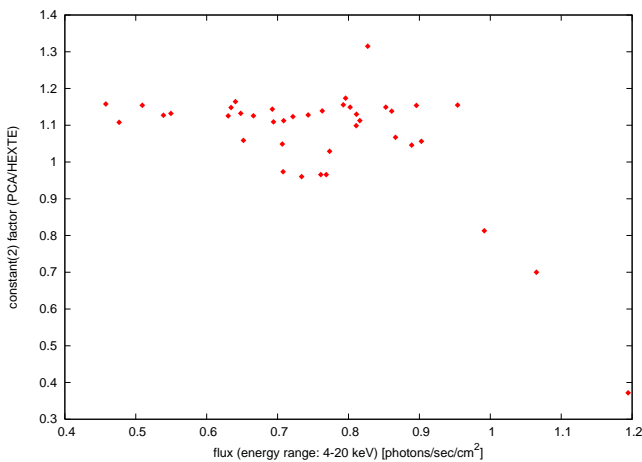FIG. 16: The total area of the Fe Kα line as a function of the photon index Γ_1.

FIG. 17: The dependence of the constant factor, which matches *PCA* data and *HEXTE* data, on the flux.

index Γ_1, which characterizes the soft state.

Another interesting point is the relation between the photon indices Γ_1, Γ_2. It can be seen in Fig. 10 that Γ_2 seems to be a linear function of Γ_1. Also in this case, the results coincide with the ones of Wilms et al. [1] (see Fig. 11). The cutoff energy averages about 27 keV. There is no obvious dependence on other parameters.

It should be noted, that the best fits for soft states could be achieved by modifying the constant factor,

which normalizes the *PCA* data to the data obtained by *HEXTE*. An explanation for this observation could be the dead time of *PCA*. To analyze this phenomenon further, the flux was calculated and the constant factor was plotted as a function of the flux. The result is shown in Fig. 17.

VI. CONCLUSION

In this work it was shown that Cyg X-1 was in a hard state, during the second half of 2005. Unfortunately there was only one observation available, which has been taken in the first half of that year. Also the small number of soft state spectra was not sufficient to confirm the hypothesis, that dead time has to be taken into account for *PCA*, when the photon flux increases in the case of a soft state. Nevertheless the relations between the fit parameters were consistent with the results of Wilms et al. [1]. This is an important point, because fixed dependences between the parameters are very helpful to find out the physics of black holes and especially BHBs, for example the accreation mechanism, the exact geometry of the corona and the disk, or the Comptonization.

[1] J. Wilms, M. A. Nowak, K. Pottschmidt, G. G. Pooley & S. Fritz 2006, A&A 447, 245-261

[2] T. Belloni 2004, Nucl. Phys B (Proc. Suppl.), 132, 337

[3] J. McClintock & R. A. Remillard 2003, in Compact Stellar X-ray Sources, ed. W. H. G. Lewin, & M. van der Klis (Cambrigde: Cambridge Univ. Press), in press [arXiv:astro-ph/0306213]

[4] T. Gleissner, "X-ray and radio variability of Cygnus X-1", http://w210.ub.uni-tuebingen.de/dbt/volltexte/2004/1299/

[5] S. Markoff, M. Nowak, S. Corbel, R. Fender & H. Falcke 2003, A&A, 397, 645

[6] J. B. Dove, J. Wilms & M. C. Begelman 1997a, ApJ, 487, 747

[7] J. B. Dove, J. Wilms, M. G. Maisack & M. C. Begelman 1997b, ApJ, 487, 759

[8] A. Herrero, R.P. Kudritzki, R. Gabler, et al., 1995, A&A 297, 556

[9] R. Fender, 2002, arXiv:astro-ph/0109502v1

[10] J. Wilms, "Active Galactic Nuclei", http://astro.uni-tuebingen.de/~wilms/teach/agn/index.html

[11] J. C. Houck and L. A. Denicola, *ISIS: An Interactive Spectral Interpretation System for high resolution X-ray spectroscopy* in proceedings of *ASP Conf. Ser. 216: Astronomical Data Analysis Software and Systems IX*, vol. 9, 2000, p. 591.

[12] Arnaud, K.A., 1996, Astronomical Data Analysis Software and Systems V, eds. Jacoby G. and Barnes J., p17, ASP Conf. Series volume 101. http://heasarc.gsfc.nasa.gov/docs/xanadu/xspec/

[13] Michael A. Nowak, http://arxiv.org/PS_cache/astro-ph/pdf/0611/0611909v1.pdf

[14] R.E. Rothschild, P.R. Blanco, D.E. Gruber, et al., 1998, ApJ 496, 538

[15] D.B. Friend, J.I.Castor, 1982, ApJ 261, 293